MODELING OF SQUAT SHEARWALLS CONTROLLED BY SHEAR

Leonardo M. Massone[1], Kutay Orakcal[2], and John W. Wallace[3]

[1] *Assistant Professor, Department of Civil Engineering, University of Chile, Santiago, Chile*
[2] *Assistant Professor, Department of Civil Engineering, Boğaziçi University, Istanbul, Turkey*
[3] *Professor, Department of Civil & Envr. Engr., University of California, Los Angeles, California, USA*
Email: lmassone@ing.uchile.cl, kutay.orakcal@boun.edu.tr, wallacej@ucla.edu

ABSTRACT :

Reinforced concrete squat walls are common in low-rise construction and as wall segments formed by window and door openings in perimeter walls. Existing approaches used to model the lateral force versus deformation responses of walls, typically assume uncoupled axial/flexural and shear responses. A more comprehensive modeling approach, which incorporates flexure-shear interaction, is implemented, validated, and improved upon using test results. The experimental program consisted of reversed cyclic lateral load testing of three-quarter scale, heavily-instrumented, wall segments dominated by shear behavior. Model results indicate that variation in the assumed transverse normal stress or strain distribution produces important response variations. Use of the average experimentally recorded transverse normal strain data, or a calibrated analytical expression for the horizontal strain, resulted in better predictions of shear strength and lateral load-displacement behavior, as did incorporating a rotational spring at wall ends to model extension of longitudinal rebar within the pedestals.

KEYWORDS: shear strength, squat wall, spandrel, pier, reinforced concrete, experiment

1. INTRODUCTION

Squat walls are very common in low-rise construction and at lower levels of tall buildings (e.g., parking level walls or basement walls). They can be also found in long walls with perforations due to window and door openings, resulting in wall segments between openings. Design of wall elements is usually oriented towards supplying sufficient shear strength to promote flexural yielding; therefore, a model that appropriately accounts for nonlinear flexural behavior is required. For low-aspect ratio walls, behavior is often dominated by nonlinear shear responses and the modeling parameters selected for shear stiffness and strength can have a significant impact on the predicted distribution of member forces and on building lateral drift.

According to experimental evidence, flexural and shear deformation interaction exists even for relatively slender walls with aspect ratio of three to four, with shear deformations contributing approximately 30% and 10% of the first story and roof level lateral displacement, respectively (Massone and Wallace, 2004). The degree of interaction for smaller aspect ratios is unclear. There is a need for relatively simple modeling approaches which consider interaction between flexure and shear responses, and capture important response features. Although a relatively large number of wall tests are reported in the literature, the primary focus for most of these tests is the assessment of wall shear strength and lateral displacement response, as opposed to assessment of relative contributions of flexural, and shear deformations to wall lateral displacements, which is necessary for validating existing and developing new modeling approaches. Therefore, experimental studies that incorporate very detailed instrumentation layouts are needed to allow development and verification of new modeling approaches.

2. MODEL DESCRIPTION AND BACKGROUND

An analytical model that couples wall flexural and shear responses was proposed by Massone (2006) and Massone et al. (2006) based on framework proposed by Petrangeli et al. (1999). The model incorporates RC panel behavior

into a two-dimensional macroscopic fiber model (Multiple Vertical Line Element Model, MVLEM (e.g., Orakcal et al., 2004), Fig. 1(a)), in order to capture the experimentally observed shear-flexure interaction in RC walls (Massone and Wallace, 2004). The model formulation involves modifying the MVLEM by assigning a shear spring to each macro-fiber of the MVLEM element (Fig. 1(b)). Each macro-fiber is then treated as a RC panel element, subjected to membrane actions, i.e., in-plane uniform normal and shear stresses (Fig. 1(b)). Therefore, the interaction between flexure and shear is incorporated at the fiber level. To represent constitutive panel behavior, a rotating-angle modeling approach, such as the Modified Compression Field Theory (MCFT, Vecchio and Collins, 1986) or the Rotating-Angle Softened-Truss-Model (RA-STM, Pang and Hsu, 1995), can be used, among other models. For each constitutive RC panel element, a uniaxial constitutive stress-strain model for concrete is applied along the principal directions to obtain the stress field associated with the principal directions, assuming that the principal stress and strain directions coincide (Vecchio and Collins, 1986; Pang and Hsu, 1995). For reinforcing steel, a uniaxial constitutive stress-strain model is applied in the directions of the reinforcing bars. Accordingly, the axial and shear responses of each fiber (panel) element are coupled, which enables coupling of flexural and shear responses of the MVLEM, since the axial response of the uniaxial elements constitute the overall flexural response of each MVLE.

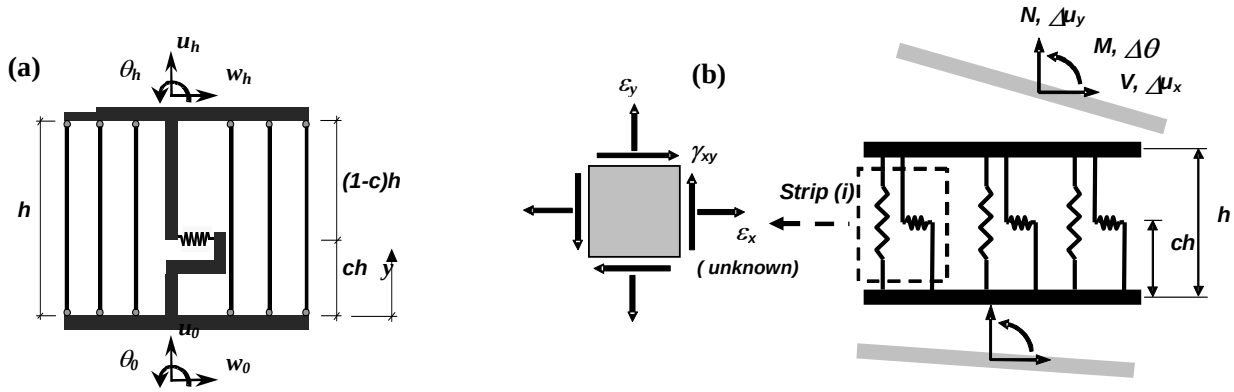

Figure 1 Element models: (a) MVLEM element and (b) coupled model element

As described by Massone et al. (2006), the deformations or strains within the components of each panel element are determined from the six prescribed degrees of freedom, (u_x, u_y and θ at both ends of the model element) as shown in Fig. 1(b). Assuming that the shear strain is uniform along the section and that plane sections remain plane, the longitudinal normal (axial) strain (ε_y) and shear distortion (γ_{xy}) components of the strain field are calculated for the entire section (for all the strips (i)) based on the prescribed degrees of freedom for the current analysis step. The transverse normal strain within each strip (ε_x) is initially estimated to complete the definition of the strain field, allowing stresses and forces to be determined from the constitutive material relationships and geometric properties (dimensions and reinforcement and concrete areas for each strip). A numerical solution procedure (e.g., Newton-Raphson method) can be employed to linearize the equilibrium equation and iterate on the unknown quantity ε_x (transverse normal strain in each strip i), to achieve horizontal equilibrium for a given resultant transverse normal stress, σ_x (resultant of transverse normal stress components in concrete and reinforcing steel), within each strip. In the case where the transverse normal strains are known, this iteration is not required. As an initial approximation in development of the model, the transverse normal stress σ_x within each strip was assumed to be equal to zero, which is consistent with the boundary conditions at the sides of a wall with no transverse loads applied over its height.

Transverse normal strains experienced along the length of the wall are significantly reduced for low aspect ratio walls, especially in regions close to the top and bottom of the wall due to the constraining effect of pedestal used at the wall ends required for testing. Thus, using an assumption of zero transverse normal strain ($\varepsilon_x = 0$), as an alternative formulation, may be more appropriate than assuming zero resultant transverse normal stress along the entire height of a wall. Comparing predictions of the two alternative model formulations ($\sigma_x = 0$, $\varepsilon_x = 0$), studies by Massone et al. (2006) revealed that neither model formulation is capable of correctly reproducing the experimental responses observed in walls with low shear span-to-depth ratios (lower than 0.5). Therefore, a more detailed description of the distribution of transverse normal strains or stresses, or variation of other model

parameters, was necessary to accurately predict the responses of such squat walls, for which well instrumented test specimens are required. The following section describes a test program with heavily-instrumented specimens, which provided the data needed to gain insight into the validity of various model assumptions.

3. TEST PROGRAM

3.1. Specimen description

The experimental program involved testing of fourteen (14), wall pier (WP) and spandrel specimens (WS), with dimensions, reinforcement configurations, and material properties selected to be representative of perimeter wall segments constructed in California between approximately 1940 and 1970. The wall segments tested were 3/4-scaled replicas. The spandrel specimens were 152 cm (60 in) tall, 152 cm (60 in) long, and 15 cm (6 in) thick, and the piers were 122 cm (48 in) tall, 137 cm (54 in) long, and 15 cm (6 in) thick with a shear-span-to-depth ratio (*M/(Vl)*) of 0.5 and 0.44, respectively. Relatively low shear span-to-depth ratios were achieved during testing of these specimens via fixing the base of the walls, restraining rotations at the top of the walls. The distributed reinforcing steel ratios of the specimens in longitudinal and transverse directions (ρ_l and ρ_t), the corresponding boundary reinforcement ratio (ρ_b), and the axial load levels applied on the specimens during the tests, as well as other specimen characteristics are presented in Table 3.1.

The test specimens included some specific features observed in older buildings, such as a weakened plane joint (WPJ) in the spandrels, where the concrete thickness is reduced and web reinforcement is cut to provide a crack initiator, and lack of hooks on horizontal web reinforcement for piers and selected spandrels. A detailed description of the experimental program and results can be found elsewhere (Massone, 2006).

Table 3.1 Properties of wall spandrel (WS) and wall pier (WP) specimens

Specimen		Test	t_w	l_w	h_w	M/(Vl$_w$)	Transverse Web Reinf.			Longitudinal Web Reinf.			Boundary Reinf.		Axial Load	Material properties (MPa)		
ID No.	Type	No.	(cm)	(cm)	(cm)		Rebar[1]	ρ_t (%)	Hooks	Rebar[1]	ρ_l (%)	Cut Bars	Rebar[1]	ρ_b (%)	N/A$_g$f'$_c$ (%)	f'$_c$	f$_y$, ϕ13	f$_y$, ϕ16
WS-T1-S1	1	test1	15.2	152	152	0.50	ϕ13@33cm	0.278	Yes	ϕ13@23cm	0.428	4 of 6[2]	4-ϕ16	3.12	0	25.5	424.0	448.2
WS-T1-S2		test4	15.2	152	152	0.50	ϕ13@33cm	0.278	Yes	ϕ13@23cm	0.428	4 of 6[2]	4-ϕ16	3.12	0	43.7	424.0	448.2
WS-T2-S1	2	test2	15.2	152	152	0.50	ϕ13@33cm	0.278	Yes	ϕ13@23cm	0.400	4 of 6[2]	1-ϕ13 + 1-ϕ16	1.70	0	31.4	424.0	448.2
WS-T2-S2		test3	15.2	152	152	0.50	ϕ13@33cm	0.278	Yes	ϕ13@23cm	0.400	4 of 6[2]	1-ϕ13 + 1-ϕ16	1.70	0	31.0	424.0	448.2
WS-T3-S1	3	test11	15.2	152	152	0.50	ϕ13@28cm	0.278	No	ϕ13@28cm	0.256	2 of 4[2]	2-ϕ13	1.33	0	31.7	351.6	-
WS-T3-S2		test14	15.2	152	152	0.50	ϕ13@28cm	0.278	No	ϕ13@28cm	0.256	2 of 4[2]	2-ϕ13	1.33	0	33.6	351.6	-
WS-T4-S1	4	test12	15.2	152	152	0.50	ϕ13@28cm	0.278	No	ϕ13@28cm	0.256	2 of 4[3]	2-ϕ13	1.33	0	31.9	351.6	-
WS-T4-S2		test13	15.2	152	152	0.50	ϕ13@28cm	0.278	No	ϕ13@28cm	0.256	2 of 4[3]	2-ϕ13	1.33	0	33.0	351.6	-
WP-T5-N0-S1	5	test9	15.2	137	122	0.44	ϕ13@30.5cm	0.278	No	ϕ13@33cm	0.227	-	2-ϕ13	1.33	0	29.9	424.0	-
WP-T5-N0-S2		test10	15.2	137	122	0.44	ϕ13@30.5cm	0.278	No	ϕ13@33cm	0.227	-	2-ϕ13	1.33	0	31.0	424.0	-
WP-T5-N5-S1		test7	15.2	137	122	0.44	ϕ13@30.5cm	0.278	No	ϕ13@33cm	0.227	-	2-ϕ13	1.33	5	31.9	424.0	-
WP-T5-N5-S2		test8	15.2	137	122	0.44	ϕ13@30.5cm	0.278	No	ϕ13@33cm	0.227	-	2-ϕ13	1.33	5	32.0	424.0	-
WP-T5-N10-S1		test5	15.2	137	122	0.44	ϕ13@30.5cm	0.278	No	ϕ13@33cm	0.227	-	2-ϕ13	1.33	10	28.3	424.0	-
WP-T5-N10-S2		test6	15.2	137	122	0.44	ϕ13@30.5cm	0.278	No	ϕ13@33cm	0.227	-	2-ϕ13	1.33	10	31.4	424.0	-

[1] ϕ13 (13 mm diameter) = US #4; ϕ16 (16 mm diameter) = US #5; [2] Weakened plane joint at wall midheight; [3] Weakened plane joint at wall-pedestal interface

3.2. Instrumentation

Each test specimen was provided with a very detailed set of instrumentation to enable post-test studies focused on model development and validation. DC-LVDTs (DC-excited linear variable differential transducer, referred to as DCDTs) were mounted on the specimens to provide measurements of average deformations at specified locations. DCDTs were located to determine overall deformations as well as local deformations to assess, for example, the contribution of shear and flexural deformations to the relative lateral displacement over the specimen height. Additional DCDTs also were mounted on the specimen to obtain average shear, transverse normal, and longitudinal normal strains.

4. ANALYTICAL MODELING STUDIES

An overview of the analytical modeling studies and comparisons with experimental results for four spandrel specimens (Tests 1 to 4), and five pier specimens (Tests 5 to 9) are presented. Results for the remaining spandrel specimens (Tests 11 to 14) are not included here, since they did not include sufficient instrumentation required for this paper. Test 10 is not included since the pier specimen was accidentally damaged prior to testing.

The shear-flexure interaction model previously described is initially used to predict the response of each wall specimen. The analysis considers monotonic lateral loading, with a zero-rotation kinematic boundary condition enforced at the top and bottom of the wall, whereas the vertical and lateral displacements at the top of the wall are not restrained. The axial load applied at the top of each wall model corresponds to the resultant of the forces applied by the vertical actuators and the self-weight of the steel reaction frame (approximately 53 kN [12 kips]). The constitutive material models were calibrated to match the as-tested material properties (concrete and steel), as described by Massone et al. (2006). In the analytical models used to represent the test specimens, 7 model elements were stacked along the height of the wall, where each model element consisted of 8 strips (panel elements) along wall length. Steel reinforcement was assumed to be distributed uniformly within each strip.

The presence of the weakened plane joint (WPJ) and the discontinuity of the longitudinal web reinforcement at the WPJ on the spandrel specimens, were not considered in the analysis, as well as, the lack of hooks on the transverse web reinforcement of the pier specimens.

4.1. Model Results - Zero Transverse Normal Stress or Strain

In this section, the model formulation described previously, which assumes zero transverse normal stress resultant ($\sigma_x = 0$) or zero transverse normal strain ($\varepsilon_x = 0$) are considered for analysis.

4.1.1 Lateral load vs. top displacement response

For all specimens, the experimentally-measured load-displacement response falls in between the upper and lower bound analytical responses predicted by the shear-flexure interaction models with zero transverse normal strain and zero transverse normal stress assumptions, respectively. In addition, the flexural model predictions for the wall lateral load capacity and stiffness are significantly larger than that for the shear-flexure interaction model predictions and the test results. This is consistent with the observed shear failure (diagonal tension and web crushing) of the test specimens.

The lateral load capacities predicted by the interaction models are compared with the experimentally-observed capacities (expressed as a ratio) in Fig. 2. As expected, the two extreme interaction model formulations (with the $\varepsilon_x = 0$ and $\sigma_x = 0$ assumptions) provide upper and lower-bound load-displacement response predictions and lateral strength predictions.

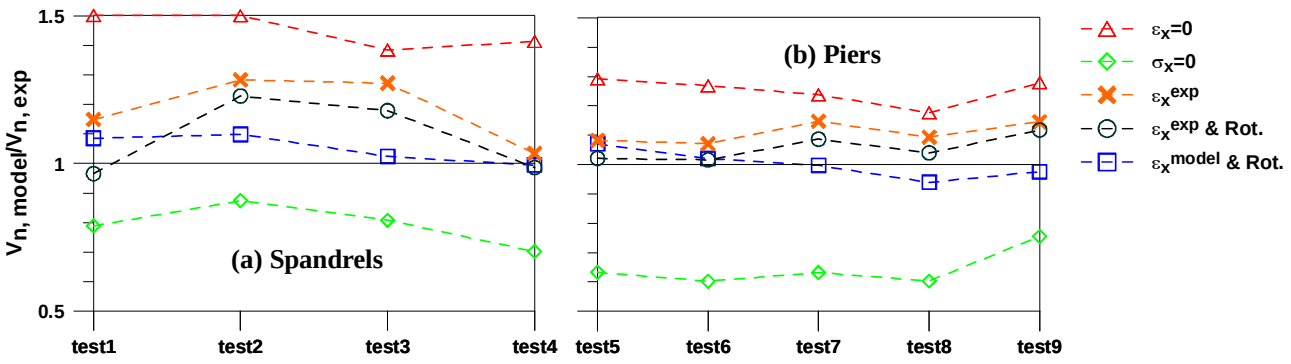

Figure 2 Relative lateral load capacity ($V_{n,model}/ V_{n,exp}$): (a) spandrels, and (b) piers

4.1.2 Flexural and shear deformation components

With either model formulation, significant inconsistencies are noted between model and experimental results for the relative contribution of flexural and shear deformations to the overall lateral displacement.

4.2. Model Results – Measured Average Transverse Normal Strains

To assess whether incorporating a more realistic transverse normal strain distribution would improve the accuracy of the analytical model, the distribution of the measured transverse normal strains obtained from test results was implemented into the model formulation. The distribution of transverse normal strains was obtained from the wall segment tests using data measured from DCDTs mounted at seven levels over the wall height. Model results obtained using the measured average transverse normal strain distributions for the peak (load reversal) points for each positive and negative loading cycle are denoted as ε_x^{exp} in several figures.

4.2.1 Lateral load vs. top displacement response

The model incorporating the experimental transverse normal strain profiles produces improved results for lateral load vs. top displacement behavior, with the predicted load-displacement responses falling in between the upper and lower bound model results (ε_x = 0 and σ_x = 0). As observed in Fig. 2, the model with the measured horizontal normal strains provides a more accurate capacity prediction than the models with upper and lower bound assumptions (ε_x = 0 and σ_x = 0, respectively). Although the model results are improved, the analytical model tends to over estimate both the lateral stiffness and the lateral load capacity of the test walls at all lateral displacement levels (e.g., Fig. 3).

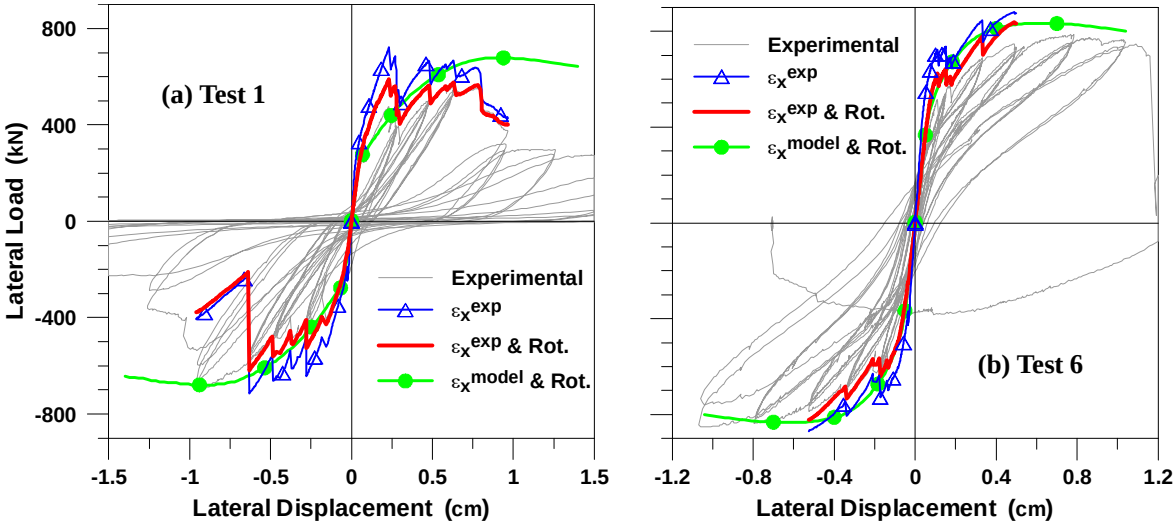

Figure 3 Load vs. top displacement (selected displacement range): (a) Test 1, and (b) Test 6

4.2.2 Flexural and shear deformation components

As shown in Fig. 4, the model results indicate that the flexural deformation component contributes significantly less to the top displacement and matches the experimental results reasonably well. Although the initial shear stiffness for the model is close to the experimental stiffness (Fig. 4(a)), for most cases, the flexural stiffness is over predicted (Fig. 4(b)).

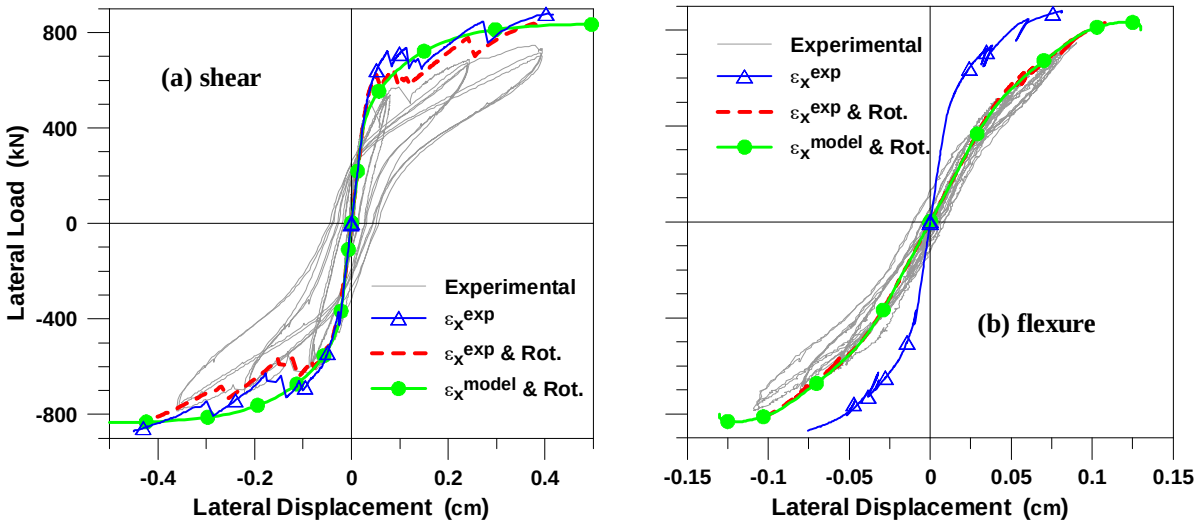

Figure 4 Load vs. top displacement: Test 6. (a) Shear, and (b) flexure

4.3. Model Results - Wall-Pedestal Interface Rotational Spring

The experimental lateral load vs. top displacement responses tend to be softer than the model predictions that incorporate measured average transverse normal strains (ε_x^{exp}), especially for the flexural deformations (Figs. 3 and 4(b)). A review of the experimental results reveals that the contribution of flexural deformations to the top displacement is concentrated within the first pair of sensors (gauge length for these sensors is 7.6 mm) located at the boundaries of the test specimens at low drift levels. Given that these sensors span the wall-pedestal interface, the potential contribution of the extension of the longitudinal reinforcing bars within the pedestals to lateral displacements measured over the wall height, was investigated.

To model the potential impact of rebar extension within the pedestals, an initial moment-curvature analysis was conducted at the wall-pedestal interfaces, assuming that a crack forms along the entire length of the interface between the specimen and the pedestals. Interface cracks, formed during post-tensioning of anchor bars or micro-cracking caused by differential shrinkage of concrete at the interfaces, were observed in several specimens. A linear strain distribution was assumed along the embedment length of the longitudinal bars within the top and bottom pedestals, with maximum strains developed at the interface and zero strain at a distance equal to the development length of the bar from the interface. The axial strains in the longitudinal bars within the pedestals were integrated to obtain cumulative displacements (bar extension) at the interface, which were converted into interface rotations (via dividing by the neutral axis depth), and used to calibrate the linear elastic stiffness (moment/rotation) of the interface rotational springs.

4.3.1 Lateral load vs. top displacement response

Implementation of the interface springs improves the agreement between the model response prediction and the experimental results for both lateral stiffness and lateral load capacity (see Fig. 3, denoted in the figure as ε_x^{exp} *& Rot.*). Peak strength predicted using the model with the interface rotational springs is about 5% to 10% lower than the model without the interface rotational springs, and better represents the experimental results (Fig. 2).

4.3.2 Flexural and shear deformation components

As expected, the model formulations that include the interface rotational springs provide significantly improved correlation (see Fig. 4). The initial shear and flexural stiffness predicted by the model that incorporates interface rotational springs (ε_x^{exp} *& Rot.*) is in good agreement with experimental results.

4.4. Model Improvements – Analytical Strain Distribution Functions

In this section, a curve-fitting approach is used to develop a general model formulation that captures the distribution of average measured transverse normal strains. It is noted that this approach can only be validated using the limited geometries of the test program described herein; therefore, the objective was to assess the potential of the approach.

4.4.1 Average horizontal normal strains

The experimental results for the spandrel and pier specimens indicated that the average horizontal normal strains generally reach a maximum value at wall mid-height, and progressively diminish to near zero at the top and bottom boundaries of the walls. As well, the magnitude of the average transverse normal strains increase with the lateral drift applied on the walls. Based on these observations, a function was used to account for the shape of the horizontal normal strains over the wall height, and another function was used to relate the maximum value of horizontal normal strain at wall mid-height to the top displacement or drift of the wall.

In order to define the relative variation of the strain values over the wall height, horizontal normal strain measurements corresponding to the seven instrumented levels on the pier and spandrel specimens were compared to the strain values measured at mid-height. A linear relationship was fitted between the data for each level and the mid-height data for all pier or spandrel specimens, to establish multipliers for all levels to relate empirically the transverse normal strain distribution along the height of the wall to the strain measurement at wall mid-height. The distribution of the average transverse normal strain coefficients at the seven levels along the height of the wall is well represented by the following best-fit expression:

$$\frac{\varepsilon_x(y)}{\varepsilon_x(h/2)} = \sin^{\alpha}\left(\frac{y}{h}\pi\right) \tag{4.1}$$

where ε_x is the horizontal normal strain at a specific position (level) along the height of the wall, y is the distance from that specific position to the bottom boundary of the wall, h is the wall height, and α is a parameter to be calibrated. Based on results of best-fit analyses, α values were determined to be 0.7 and 0.4 for the spandrel and pier specimens, respectively.

The defined distribution of the average transverse normal strains is normalized with respect to the strain value at wall mid-height, which also needs to be characterized. The data from all specimens show a similar relationship between mid-height strain and top displacement, with no significant variation between the spandrels and the piers. Thus, a single expression (function) was selected to relate the average normal strain at the mid-height to the top displacement for all specimens. The relationship was represented by the following expression:

$$\varepsilon_x(h/2, \Delta) = 0.0045\Delta^{1.6} \tag{4.2}$$

where $\varepsilon_x(h/2)$ is the horizontal normal strain at wall mid-height and Δ is the lateral top displacement (cm) of the wall.

4.4.2 Lateral load vs. top displacement response

According to Fig. 3, the model with analytical average horizontal normal strains and rotational interface springs (denoted in the figure as ε_x^{model} *& Rot.*) predicts, with reasonable accuracy, the experimental load-displacement response, providing a reasonably good representation of not only the lateral load capacity, but also the lateral stiffness of the walls. Compared to all of the previous model implementations, the present model (with the analytical horizontal normal strains) provides an improved overall capacity prediction (Fig. 2), with the error in the prediction not exceeding 10% for all individual specimens.

4.4.3 Flexural and shear deformation components

The initial shear stiffness predicted by all models is in good agreement with the experimental results (Fig. 4). The flexural stiffness predictions also compare favorably with the experimental results provided the rotational interface springs are incorporated.

5. SUMMARY AND CONCLUSIONS

This study investigated and verified experimentally a modeling approach that integrates flexure and shear interaction for a reliable prediction of the inelastic response of reinforced concrete squat walls. The model incorporates RC panel behavior described by a rotating-angle approach, similar to the RA-STM into the fiber-based Multiple Vertical Line Element Model (MVLEM). The experimental program carried out as part of this study was used to improve the predictions of the model by modifying some of the model assumptions.

The experimental results showed that the wall ends (pedestal and beam) constrained the transverse normal strain, which was not considered in the original interaction model. The model with zero resultant horizontal stress (σ_x = 0) or zero horizontal strain (ε_x = 0) assumption resulted in a softer or stronger load – displacement relation.

The overall load-displacement responses obtained from the model were improved, resulting in an overestimate of the experimental shear capacity by 3 to 28% by using the experimentally measured average transverse normal strain. Although, the model shear strength was close to the experimental measured strength, the stiffness measured during the experiments was less than obtained using the model. This discrepancy, attributed to rotations at the wall-end interfaces due to rebar extension (pedestal), was accounted for with an additional rotational flexibility that resulted in improved correlation between model and experimental results for stiffness and strength.

Based on the findings from this experimental program, an average transverse normal strain equation (and distribution function) was calibrated to investigate the potential of improving the shear-flexure interaction model. A good correlation was obtained for shear capacity and shear and flexural components of top displacement. The experimental shear capacity was estimated with an error of about 10% for individual specimens.

REFERENCES

Massone, L. M., and Wallace, J. W. (2004). Load – deformation responses of slender reinforced concrete walls. *ACI Structural Journal* **101:1**, 103-113.
Massone, L. M. (2006). RC Wall Shear – Flexure Interaction: Analytical and Experimental Responses. *Ph.D. Dissertation*, University of California, Los Angeles.
Massone, L. M., Orakcal, K., and Wallace, J. W. (2006). Shear - Flexure Interaction for Structural Walls. SP-**236**, ACI Special Publication – *Deformation Capacity and Shear Strength of Reinforced Concrete Members Under Cyclic Loading*, editors: Adolfo Matamoros & Kenneth Elwood, 127-150.
Orakcal, K., Wallace, J. W., and Conte, J. P. (2004). Nonlinear Modeling and Analysis of Slender Reinforced Concrete Walls. *ACI Structural Journal* **101:5**, 688 - 699.
Petrangeli, M., Pinto, P. E., and Ciampi, V. (1999). Fiber Element for Cyclic Bending and Shear of RC Structures. I: Theory. *Journal of Engineering Mechanics* **125:9**, 994-1001.
Vecchio, F. J., and Collins, M. P. (1986). The Modified Compression-Field Theory for Reinforced Concrete Elements Subjected to Shear. J*ournal of the American Concrete Institute* **83:2**, 219-231.
Pang, X. D., and Hsu, T. T. C. (1995). Behavior of Reinforced Concrete Membrane Elements in Shear. *ACI Structural Journal* **92:6**, 665-679.